EXPERIMENTAL AND THEORETICAL STUDY OF FAILURE OF CERAMIC BRICK

Andrzej LITEWKA[*], Leszek SZOJDA[**]

[*] Departamento da Engenharia Civil, Universidade da Beira Interior, Calçada Fonte do Lameiro, 6200-358 Covilhã, Portugal
[**] Department of Civil Engineering, Silesian University of Technology, ul. Akademicka 5, 44-100 Gliwice, Poland

litewka@ubi.pt

Abstract: The aim of the paper is to present experimental and theoretical study of deformability and fracture of brittle rock-like materials. To this end the tests of the specimens of ceramic brick subjected to various combinations of tri-axial state of stress components were performed. These experiments made it possible to construct the stress-strain curves and to measure the stresses at material failure. The data obtained for uni-axial compression were used to determine the constants included
in the theoretical model. All the experimental data obtained for tri-axial loading were compared with the theoretical predictions.

1. INTRODUCTION

Complexity of phenomena that affect mechanical res-ponse of brittle rock-like materials give rise to suitable ex-periments on deformability, damage growth and fracture of rocks, cementitous composites and ceramics. Some results of experimental studies of mechanical behaviour of such materials have been previously reported mainly for uni-axial and bi-axial loading of concrete (Kupfer, 1973). The expe-rimental data for rocks and concrete subjected to tri-axial state of stress are presented by Cristescu and Hunsche (1998), Chen (1982) and Neville (1995). Simultaneously new approach based on the methods of continuum damage mechanics has been used to formulate phenomenological models capable to describe the mechanical behaviour of brittle rock-like materials (Litewka et al., 1996; Murakami and Kamiya, 1997; Halm and Dragon, 1998). Because of limited experimental data available, particularly these for tri-axial state of stress, all the theoretical descriptions were verified for some specific cases of loading only. To obtain more realistic theoretical description of overall material response further extensive experimental studies are needed.

The aim of this paper is to supply experimental data on deformability and fracture of ceramic brick subjected to tri-axial state of stress as well as to show potentialities of own theoretical model (Litewka et al., 1996; Litewka and Dębiński, 2003). The experiments presented in this note for two different types of brick have been projected as a conti-nuation of those described elsewhere (Litewka and Szojda, 2006) for only one type of brick.

2. EXPERIMENTS

The results presented here were obtained for two different sets of the brick specimens referred to as Brick 1 and Brick 2. The specimens of Brick 1 were cut out of the same material that was analyzed by Litewka and Szojda (2006) and that is why the recent and older data can be compared. The height and diameter of the cylindrical spe-cimens (Fig. 1) cut out from standard plain brick were equal to 12 cm and 6 cm, respectively. The details of the speci-mens preparation and the experimental procedure can be found elsewhere (Szojda, 2001).

The tests were performed for uni-axial compression and for two cases of tri-axial compression explained in Fig. 1 and referred to as State I and State II. The objective of the test performed under uni-axial compression was to calibrate the materials. That is why the initial Young modulus E_0 and Poisson ratio ν_0 as well as uni-axial compressive strength f_c were measured experimentally for both materials tested. The data shown in Table 1 were cal-culated as mean values of those measured for seven speci-mens of Brick 1 and for three specimens of Brick 2. The values of standard constants E_0, ν_0, f_c and those for five other parameters A, B, C, D and F seen in Table 1 are necessary to employ the theoretical model presented by Litewka & Dębiński (2003).

The objective of the tests under tri-axial state of stress was to measure the stresses at material fracture for pres-cribed loading programs. It is seen from Fig. 1 that the tri-axial State I is a combination of uni-axial compression and hydrostatic pressure whereas the State II is a simultaneous

Tab. 1. Material constant for brick

Constant	Unit	Material	
		Brick 1	Brick 2
E_0	MPa	2550	9390
ν_0	-	0.103	0.126
f_c	MPa	-10.85	-28.78
A	MPa^{-2}	1064×10^{-5}	170.2×10^{-5}
B	MPa^{-2}	100.0×10^{-5}	31.75×10^{-5}
C	MPa^{-1}	-1.500×10^{-5}	-0.1201×10^{-5}
D	MPa^{-1}	2.800×10^{-5}	0.2403×10^{-5}
F	-	0.6900	0.6000

Tab. 2. Experimental and theoretical failure stress for Brick 1 subjected to State I of tri-axial compression.

Specimen	Hydrostatic pressure, p	Failure stress σ_{3f}	
		Experiment	Theory
	[MPa]	[MPa]	[MPa]
C2*	0	-10.24	-11.87
C3*	0	-12.59	-11.87
C4*	0	-11.65	-11.87
CC1*	-1.11	-15.34	-15.80
CC2*	-2.13	-20.86	-19.34
CC3*	-3.22	-22.25	-22.56
CD1*	-1.11	-16.59	-15.80
CD2*	-2.13	-22.05	-19.34
CD3*	-3.65	-22.96	-23.70
B1-H0-1	0	-9.36	-11.87
B1-H0-2	0	-11.93	-11.87
B1-H0-3	0	-10.27	-11.87
B1-H0-4	0	-9.29	-11.87
B1-H3-1	-3.25	-19.59	-22.63
B1-H3-2	-3.69	-21.56	-23.80
B1-H6-1	-6.64	-34.17	-30.83
B1-H6-2	-6.55	-33.66	-30.63
B1-H6-3	-6.57	-31.93	-30.67
B1-H9-2	-9.50	-38.51	-36.75
B1-H9-3	-9.34	-40.68	-36.44

* The data for these specimens of Brick 1 were discussed in Litewka & Szojda (2006).

Tab. 3. Experimental and theoretical failure stress for Brick 1 subjected to State II of tri-axial compression.

Specimen	Hydrostatic pressure, p	Failure stress $\sigma_{1f} = \sigma_{2f}$	
		Experiment	Theory
	[MPa]	[MPa]	[MPa]
CA1*	0	-10.49	-11.87
CA2*	-2.76	-21.94	-23.94
CA3*	-3.34	-24.70	-25.54
CB1*	-0.06	-14.36	-12.47
CB2*	-2.51	-17.19	-23.19
CB3*	-3.63	-22.83	-26.30
B1-V0-1	-0.14	-13.03	-13.14
B1-V0-2	-0.20	-14.18	-13.23
B1-V2-1	-1.97	-23.50	-21.51
B1-V2-2	-1.93	-23.43	-21.40
B1-V2-3	-1.97	-25.74	-21.51
B1-V3-1	-3.70	-20.86	-26.48
B1-V3-2	-3.36	-22.86	-25.58
B1-V6-1	-6.31	-30.48	-32.65
B1-V6-3	-6.44	-32.98	-32.95
B1-V9-1	-9.09	-36.21	-38.42
B1-V9-2	-9.25	-34.83	-38.77
B1-V9-3	-9.53	-31.56	-39.30

* The data for these specimens of Brick 1 were discussed in Litewka & Szojda (2006).

action of hydrostatic pressure and uniform bi-axial comp-ression. Various combinations of the stress tensor compo-nents and at least two different loading paths shown in Fig. 2 are necessary to supply information on the shape of the limit surface at failure of the material subjected to tri-axial states of stress. The loading paths for State I and State II of tri-axial state of stress consisted of two stages. The Stage 1 was the same in both cases of tri-axial loading and consisted in a monotonic increase of hydrostatic pressure up to pre- scribed value p. In the Stage 2 of the first tri-axial state of

Tab. 4. Experimental and theoretical failure stress for Brick 2 subjected to State I of tri-axial compression.

Specimen	Hydrostatic pressure, p	Failure stress σ_{3f}	
		Experiment	Theory
	[MPa]	[MPa]	[MPa]
B2-H0-1	0	-25.49	-29.68
B2-H0-2	0	-29.65	-29.68
B2-H0-3	0	-31.19	-29.68
B2-H8-2	-8.66	-57.29	-56.29
B2-H8-3	-7.74	-61.49	-53.93

Tab. 5. Experimental and theoretical failure stress for Brick 2 subjected to State II of tri-axial compression.

Specimen	Hydrostatic pressure, p	Failure stress $\sigma_{1f} = \sigma_{2f}$	
		Experiment	Theory
	[MPa]	[MPa]	[MPa]
B2-V4-1	-4.17	-43.81	-49.44
B2-V4-2	-3.83	-44.93	-48.32
B2-V6-2	-6.37	-50.68	-56.05
B2-V8-1	-7.93	-64.22	-60.25
B2-V8-2	-8.07	-50.36	-60.59

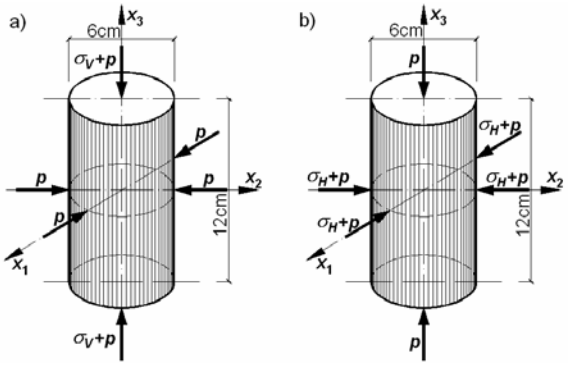

Fig. 1. Tri-axial loading of the specimens: a) State I, b) State II

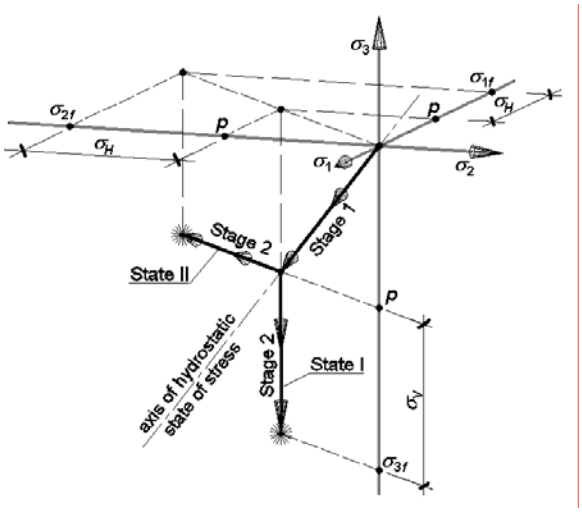

Fig. 2. Loading paths for tri-axial State I and State II: ∗ point corresponding to material fracture.

stress (State I) the compressive vertical normal stress σ_V was increased up to material failure that occurs for $\sigma_{3f} = p + \sigma_V$. In the Stage 2 of the State II of tri-axial load-ing two compressive horizontal components σ_H

of uniform bi-axial state of stress were increased simultaneously up to material failure that corresponds to $\sigma_{1f} = \sigma_{2f} = p + \sigma_H$. To obtain several combinations of the stress tensor compo-nents the various levels of the hydrostatic pressure p were used. The respective numerical data presented earlier (Litewka and Szojda 2006) as well as new ones are shown in Tables 2-5. The new experiments performed for Brick 1 and Brick 2 according to the program seen in Tables 2-5 made it possible to analyze the mechanical behaviour of brick subjected to higher levels of hydrostatic pressure p than those in earlier tests done for fifteen specimens of Brick 1 only.

3. THEORY AND DISCUSSION

The details of the theoretical model employed in this paper were presented in earlier papers (Litewka et al., 1996; Litewka and Dębiński, 2003; Litewka and Szojda 2006)
and that is why the final form of the respective relations will be shown here. This model is based on the rules of the conti-nuum damage mechanics presented by Murakami (1987). The current state of the deteriorated material structure is described by the symmetric second rank damage tensor Ω_{ij} defined by Murakami and Ohno (1981) and Betten (1983). The relevant constitutive equations were found (Litewka et al. 1996, Litewka and Dębiński 2003) by using the methods of the theory of tensor function representations applied to solid mechanics by Boehler (1987). The first equation of the theoretical model is the stress-strain relation for anisotropic elastic solid

$$\varepsilon_{ij} = -\frac{\nu_0}{E_0}\delta_{ij}\sigma_{kk} + \frac{1+\nu}{E_0}\sigma_{ij} + \\ + C\left(\delta_{ij}D_{kl}\sigma_{kl} + D_{ij}\sigma_{kk}\right) + 2D\left(\sigma_{ik}D_{kj} + D_{ik}\sigma_{kj}\right), \tag{1}$$

where ε_{ij} is the strain tensor and σ_{ij} is the stress tensor. Equ-ation (1) contains the Kronecker delta δ_{ij}, the Young mo-dulus E_0 and Poisson ratio ν_0 for an originally undamaged material, two constants C and D to be determined experi-mentally and modified damage tensor D_{ij} responsible for the current state of material structure defined by Litewka (1989).

Deterioration of the material structure due to applied load was described by the damage evolution equation ex-pressed in the form of the tensor function

$$\Omega_{ij} = \left(As_{kl}s_{kl}\delta_{ij} + B\sqrt{\sigma_{kl}\sigma_{kl}}\sigma_{ij}\right)\cdot \\ \cdot\left(1 + \frac{227\det\boldsymbol{\sigma}}{200\left|\det\boldsymbol{\sigma}\right| + \left|\left(\sigma_{pp}\right)^3\right|}\right)^F, \tag{2}$$

where Ω_{ij} is a classical second order damage tensor, s_{kl} is the stress deviator, $\det\boldsymbol{\sigma}$ is the determinant of the matrix $\boldsymbol{\sigma}$ of the stress tensor σ_{ij} and A, B, F are material parameters to be determined experimentally. The relation

$$D_i = \frac{\Omega_i}{1-\Omega_i}\ , \ i = 1, 2, 3 \tag{3}$$

between the principal values Ω_1, Ω_2 and Ω_3 of the damage tensor Ω_{ij} and the principal components D_1, D_2 and D_3 of the modified damage tensor D_{ij} contained in Eq. (1) was formulated by Litewka (1989).

Theoretical model used in this paper makes it possible to determine the maximum stresses that can be sustained by the material subjected to multi-axial state of stress. To this end the appropriate fracture criterion for brittle material was formulated according to the rules of the damage mechanics. The physical background of this criterion was looked for in the results of experiments and in the failure modes of bro-ken specimens. It was found that tri-axial compression of brittle materials results in crack growth to such a state that the net cross section area on certain planes is reduced to zero. This full deterioration of internal structure of the ma-terial occurs when at least one of the principal components Ω_1, Ω_2 or Ω_3 of the damage tensor Ω_{ij} determined from Eq. (2) reaches the limit value equal to unity.

To compare the experimental results with theoretical prediction, Eq. (2) was expressed in terms of the stress tensors components shown in Fig. 1a and the relation

$$\Omega_1 = \Omega_2 = \left(\frac{2}{3}A\sigma_V^2 + Bp\sqrt{\sigma_V^2 + 2\sigma_V p + 3p^2}\right)\cdot \\ \cdot\left[1 + \frac{227(\sigma_V + p)p^2}{200\left|(\sigma_V + p)p^2\right| + \left|(\sigma_V + 3p)^3\right|}\right]^F = 1 \tag{4}$$

was obtained for State I. The third principal component of the damage tensor Ω_3 does not decide in this case on the material fracture as it grows slower than Ω_1 and Ω_2. The State II of tri-axial compression seen in Fig. 1b is charac-terized by faster growth of the principal component Ω_3 of the damage tensor and that is why the material fracture occurs when

$$\Omega_3 = \left(\frac{2}{3}A\sigma_H^2 + Bp\sqrt{2\sigma_H^2 + 4\sigma_H p + 3p^2}\right)\cdot \\ \cdot\left[1 + \frac{227(\sigma_H + p)^2 p}{200\left|(\sigma_H + p)^2 p\right| + \left|(2\sigma_H + 3p)^3\right|}\right]^F = 1\ . \tag{5}$$

In this case two others principal components Ω_1 and Ω_2 of the damage tensor are smaller than Ω_3 and that is why they do not decide about the onset of fracture.

Application of the fracture criterion requires calibration of the material. The numerical values of the constants A, B, C, D and F shown in Table 1 were obtained by using the stress-strain curves determined experimentally for uni-axial compression of Brick 1 and Brick 2. The details of the method used to identify the material parameters have been described by Litewka and Dębiński (2003). The constant F that appears in Eqs (2), (4), (5) was also determined experi-mentally and to do this, one point taken from one stress-strain curve obtained experimentally for tri-axial compres-sion is sufficient.

Equations (4) and (5) were used to calculate the values of σ_V and σ_H corresponding to material failure in State I and

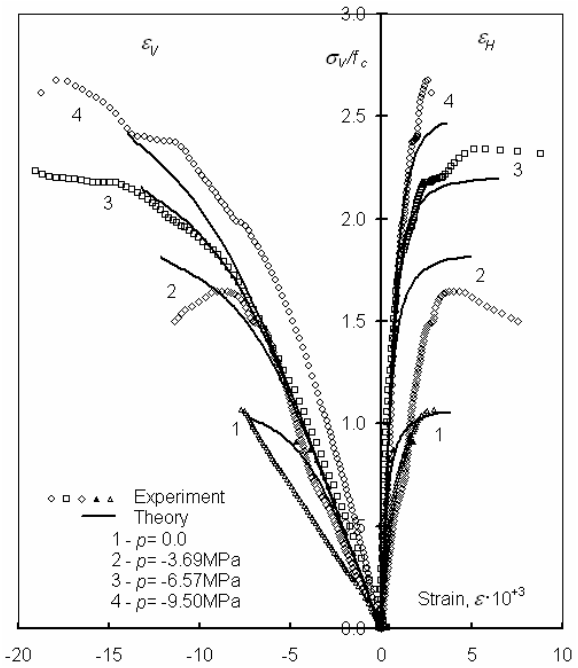

Fig. 3. Experimental and theoretical stress-strain curves for State I of tri-axial compression of Brick 1: 1 - Specimens B1-H0-3 and C4, 2 - Specimen B1-H3-2, 3 - Specimen B1-H6-3, 4 – Spe-cimen B1-H9-2

State II. These data made it possible to determine the theo-retical stresses at material fracture $\sigma_{3f} = p + \sigma_V$ for State I and $\sigma_{1f} = \sigma_{2f} = p + \sigma_H$ for State II. Comparison of these theoretical predictions with corresponding experimental da-ta is shown in Tables 2-5.

Equation (1) specified for the State I and State II of tri-axial loading explained in Fig. 1 made it possible to compare the theoretical predictions with the stress-strain relations obtained experimentally. Some examples of such curves for Brick 1 subjected to State I shown in Fig. 3 present the relation between variable component σ_V and horizontal or vertical strains determined from the relations

$$\varepsilon_V = \varepsilon_3 - \frac{1-2\nu_0}{E_0} p\,, \quad \varepsilon_H = \varepsilon_1 - \frac{1-2\nu_0}{E_0} p\,. \tag{6}$$

The principal strains $\varepsilon_1 = \varepsilon_2$ and ε_3 seen in Eq. (6) are measured experimentally or calculated directly from Eq. (1) for experimental or theoretical curves, respectively.

4. CONCLUSIONS

Experiments on behaviour of two types of brick sub-jected to tri-axial loading were used to study the fracture of brittle materials under higher values of compressive mean stresses than those applied in earlier tests. The theoretical stress-strain curves and stresses at material failure were determined and compared with the experimental data ob-tained. Fairly good agreement of the experimental data and theoretical predictions was detected for both materials tes-ted. Increase of compressive strength of materials for increasing hydrostatic pressure observed for both materials in both tri-axial tests used can be explained theoretically within the mathematical model proposed. Thus, the experi-mental technique adopted and phenomenological model used in this paper proved to be accurate enough to study the fracture of brittle rock-like materials.

REFERENCES

1. **Betten J.** (1983), Damage tensors in continuum mechanics, *J. Méch. Théor. Appl.*, Vol. 2, No 1, 13-32.
2. **Boehler J.P.** (1987), *Applications of tensor functions in solid mechanics*, Springer-Verlag, Wien.
3. **Cristescu N.D., Hunsche U.** (1998), *Time effects in rock mechanics*, John Wiley & Sons, Chichester.
4. **Chen W.F.** (1982), *Plasticity of reinforced concrete*, McGraw-Hill, New York.
5. **Halm D., Dragon A.** (1998), An anisotropic model of damage and frictional sliding for brittle materials, *Eur. J. Mech., A/Solids*, Vol. 17, No 3, 439-460.
6. **Kupfer H.** (1973), Das Verhalten des Betons unter mehrach-siger Kurzzeitbelastung unter besonderer Beruck-sichtigung der zweiachsiger Beanspruchung, In: *Deutcher Ausschluss fur Stahlbeton*, 229, Wilhelm Ernst & Sohn, Berlin, 1-105.
7. **Litewka A.** (1989), Creep rupture of metals under multi-axial state of stress, *Arch. Mech.*, Vol. 4l, No 1, 3-23.
8. **Litewka A., Bogucka J., Dębiński J.** (1996), Deformation induced anisotropy of concrete, *Arch. Civil Eng.*, Vol. 42, No 4, 425-445.
9. **Litewka A., Dębiński J.** (2003), Load-induced oriented damage and anisotropy of rock-like materials, *Int. J. Plast.*, Vol. 19, No 12, 2171-2191.
10. **Litewka A., Szojda L.** (2006), Damage, plasticity and failure of ceramics and cementitious composites subjected to multi-axial state of stress, *Int. J. Plast.*, Vol. 22, No 11, 2048-2065.
11. **Murakami S.** (1987), Progress in continuum damage mechanics, *JSME Int. J.*, Vol. 30, 701-710.
12. **Murakami S., Kamiya K.** (1997), Constitutive and damage evolution equations of elastic-brittle materials based on irreversible thermodynamics, *Int. J. Mech. Sci.*, Vol. 39, No 4, 473-486,.
13. **Murakami S., Ohno N.** (1981), A continuum theory of creep and creep damage, In: *Creep in Structures*, eds. A.R.S. Ponter, D.R. Hayhurst, Springer-Verlag, Berlin, 422-444.
14. **Neville, A.M.** (1995), *Properties of concrete*, Longman, Harlow.
15. **Szojda L.** (2001), *Analysis of interaction of masonry structures and deformable foundation*, PhD Thesis, Silesian University of Technology, Gliwice, (in Polish).

TEORETYCZNO-DOŚWIADCZALNE STUDIUM PĘKANIA CEGŁY CERAMICZNEJ

Streszczenie: W pracy przedstawione jest teoretyczno-doświadczalne studium odkształcalności i pękania skałopodobnych materiałów kruchych. W tym celu przeprowadzono badania próbek ce-gły ceramicznej poddanych różnym kombinacjom składowych trójosiowego stanu naprężenia. Wykonane badania umożliwiły wykreślenie krzywych ściskania oraz pomiar naprężeń niszczą-cych. Dane otrzymane dla osiowego ściskania wykorzystane zosta-ły do określenia stałych zawartych w modelu teoretycznym. Wyniki doświadczalnie otrzymane dla trójosiowego obciążenia zostały porównane z przewidywaniami teoretycznymi.

Acknowledgements: This work was done within the F.C.T. Program C.E.C. U.B.I. and was financially supported by KBN Grant 5 T07E 028 25 and EC contract MTKD-CT-2004-509775.